Behaviors of Impurity in ITER using BALDUR code

W. Buangam[1], S. Dangkong[1], J. Promping[3], B. Chatthong[1],
T. Onjun[1], N. Poolyarat[2] and R. Picha[3]

[1]*Sirindhorn International Institute of Technology, TU, Pathumthani, Thailand*

[2]*Department of Physics, Thammasat University, Pathumthani, Thailand*

[3]*Thailand Institute of Nuclear Technology, Bangkok, Thailand*

1. Introduction

Impurity is considered one of the concerned issues in plasma nuclear fusion because it can radiate energy and dilute fuel, which affects the performance of nuclear fusion. Helium ash (alpha particle) is the most obvious and most abundant impurity in fusion plasma because it is a product of deuterium-tritium (D-T) nuclear fusion reaction. Beryllium (Be), carbon (C) and oxygen (O) are also considered impurity and can be released from plasma facing components [1], [2], [3]. In addition, plasma facing components made of lithium can reduce the flux of recycled particles entering the plasma edge from the plasma facing components [4]. Unlike other impurities, nitrogen (N) and neon (Ne) are extrinsic impurity. The work of Schweinzer *et al*. [5] shows that an injection of nitrogen can reduce the thermal load on the diverter by radiating the power to the main chamber, while the work of Beurskens *et al*. [6] shows that an appropriate injection of neon can reduce the ELM energy loss. As a result, it is crucial to investigate these impurities behavior in ITER, especially the impurity transport and accumulation. The accumulation of these impurities can cause many problems such as core radiation enhancement, fuel dilution or even plasma disruptions [6]. In this work, we have studied the behaviors of impurity on impurity transport and accumulation in ITER by using 1.5D BALDUR integrated predictive modeling code. This paper is organized as follows: brief descriptions of relevant components of the BALDUR code, including the Multimode Core Transport Model (MMM95) and NCLASS Module given in section 2; the prediction of ITER plasma profiles are presented and discussed in section 3; and summary is given in section 4.

2. BALDUR integrated predictive modeling code

The BALDUR integrated predictive modeling code [7] has been used intensively and widely to calculate the time evolution of various tokamak plasma properties, including electron and ion temperatures, deuterium and tritium densities, helium and impurity densities. The BALDUR code self-consistently computes these profiles by mixing many physical processes together in the form of modules including transport, plasma heating, particle flux, boundary conditions and etc. It was found that the BALDUR code could yield results in a very good agreement with experimental data. For example, in [8-9], the BALDUR simulations with the MMM95 transport model yielded an agreement of about 10% relative root mean square (RMS) deviation.

2.1 Multimode Core Transport Model (MMM95)

The Multi-Mode Model version 1995 (MMM95) [10] is a combination of theory-based transport models used to predict plasma profiles in tokamaks. It consists of the Weiland model for the ion temperature gradient (ITG) and trapped electron modes (TEM), the Guzdar–Drake model for drift-resistive ballooning modes, and kinetic ballooning modes. Usually, the Weiland model for drift modes provides the largest contribution, followed by the drift- resistive ballooning mode and the kinetic ballooning mode respectively. The expressions of transport coefficients in MMM95 are:

$$\chi_i = 0.8\chi_{i,ITG\&TEM} + \chi_{i,RB} + 0.65\chi_{i,KB}$$
$$\chi_e = 0.8\chi_{e,ITG\&TEM} + \chi_{e,RB} + 0.65\chi_{e,KB}$$
$$D_H = 0.8D_{H,ITG\&TEM} + D_{H,RB} + D_{H,KB}$$
$$D_Z = 0.8D_{Z,ITG\&TEM} + D_{Z,RB} + D_{Z,KB}$$

2.2 NCLASS Module

The NCLASS module [11] calculates the neoclassical transport properties of multi-species axisymmetric plasma of arbitrary aspect ratio, geometry and collisionality. The neoclassical effects refer to the flows of Coulomb collisions between particles drifting in nonuniform magnetic and electric fields. This module determines a multifluid model for the parallel and radial force balance equations from which the neoclassical bootstrap current, parallel electrical resistivity, impurity and fuel ion radial particle transport, ion radial thermal transport and plasma poloidal rotation. It is designed to be called from a transport code that provides the plasma density and temperature profiles.

3. Simulation results and discussion

In this work, we have studied the behaviors of impurity in ITER by using 1.5D BALDUR integrated predictive modeling code. The engineering parameters for these scenarios are shown in table 1.

Table 1. The physical parameters

Parameter	Value	Unit
Major radius (R)	6.2	m.
Minor radius (a)	2.0	m.
Plasma current (I_p)	15	MA
Magnetic field (B_T)	5.3	T
Elongation (κ_{95})	1.7	-
Triangularity (δ_{95})	0.5	-
Line-average density ($\overline{n_l}$)	10^{20}	m^{-3}

Deuterium, tritium, and two species of impurity are considered as plasma in all simulations, where helium is considered as one of the impurities. Another impurity can be lithium (Li), beryllium (Be), carbon (C), nitrogen (N), oxygen (O) and neon (Ne). For each simulations, a linear combination of MMM95 anomalous transport and NCLASS neoclassical transport is used to describe both thermal and particle transports. The total auxiliary heating power used in the simulations in 40 MW, of which 33 MW comes from the neutral beam injection (NBI) heating and 7 MW comes from the ion cyclotron resonance frequency (ICRF) heating. The boundary conditions are provided at the top of the pedestal. We assume that pedestal electron temperature, which equals to 0.4 keV is the same as pedestal ion temperature while the pedestal impurity density is about 0.01% of deuterium density. The plasma evolution time in all simulations is set to be 1000 s. For the sake of computation, some physical processes are not included these simulation, such as ELM crashes and sawtooth oscillation. Thus, the simulation does not represent the complete ITER plasma dynamics. However, it is expected that these simulations would have sufficient physics to describe the plasma when it reaches steady state. In this work, the impurity influx is assumed to be 10^{15} particles/(cm^2s).

The results of simulation show that central helium concentration in low atomic number background impurities will be higher than that in a higher atomic number background impurity. This is shown in Figure 1; whereas central helium concentration in Li background is higher than central helium concentration in Be, C, N, O, and Ne. Also, a lower atomic number background impurity will reach steady state faster. It is found that a simulation with a lower atomic number impurity will give higher helium and impurity density for all regions from core to pedestal area. Furthermore, the electron and ion temperature are also higher from a lower atomic number impurity. From our simulations, this trend is also true when considering alpha power. This could be due to lower radiation loss of low atomic number impurity when comparing with higher atomic number impurity. Moreover, the decrease of impurity with the higher mass is as expected due to the increase of impurity diffusivity (D_Z). Figure 4 shows the profiles of average impurity diffusivity (D_Z) at steady state during the time 600 to 1000 s for Li, Be, C, N, O and Ne and the profiles of contributing terms of average impurity diffusivity at steady state during the time 600 to 1000 s for Li. It is found that the average impurity

diffusivity becomes larger when using impurity of higher mass. It can be seen that for D_Z, the kinetic-ballooning term (KB) is the largest contribution in the center of the plasma, the ITG term (ITG) provides the largest contribution in the region close to the center and the resistive ballooning contribution term (RB) provides the largest contribution near the edge of the plasma. It is also found the radial profiles of the KB term are similar in all impurity scenarios. The RB profiles in different impurity scenarios are similar too except for Ne case , in which the RB term provides larger contribution near the edge and decreases dramatically at the edge of plasma. It is found that the simulation with higher mass of impurity will have higher profile of ITG term.

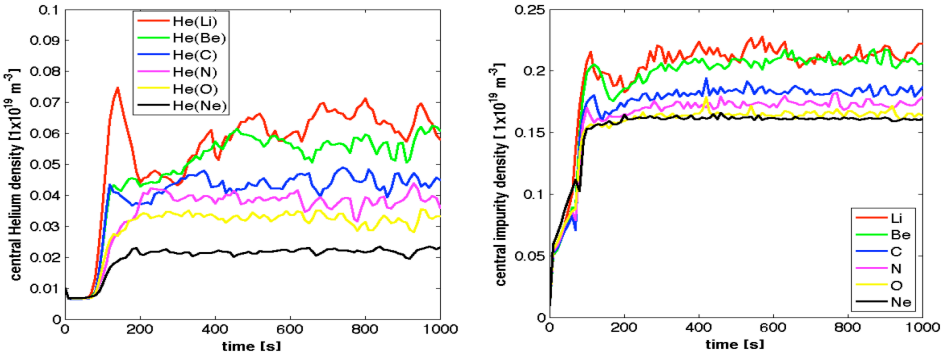

Figure 1. Time evolution of helium density at the plasma core in various background impurities (left) and those background impurities' density also at the plasma core (right).

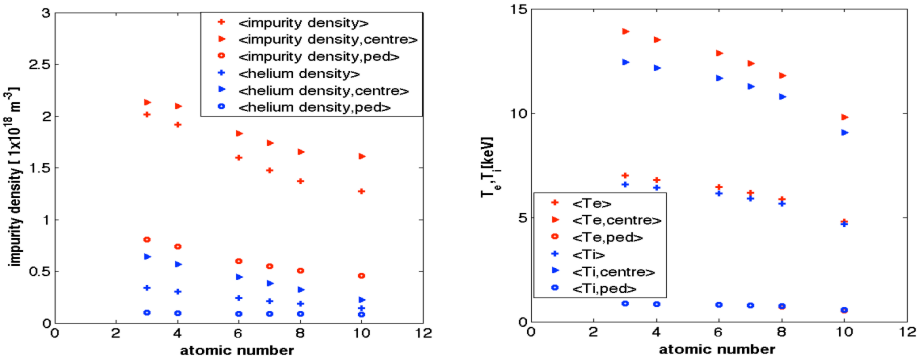

Figure 2. The average total density of impurity and helium, average central density of impurity and helium and average pedestal density of impurity and helium (left) and the average total electron temperature and ion temperature, average central electron temperature and ion temperature and average pedestal electron temperature and ion temperature (right) at steady state during the time 600 to 1000 s is plotted as a function of the atomic number of the impurity.

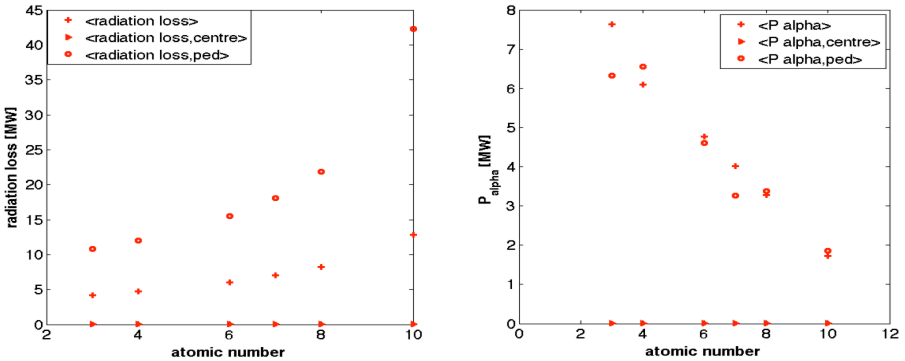

Figure 3. The average total density of impurity and helium, average central density of impurity and helium and average pedestal density of impurity and helium (left) and the average total electron

temperature and ion temperature, average central electron temperature and ion temperature and average pedestal electron temperature and ion temperature (right) at steady state during the time 600 to 1000 s is plotted as a function of the atomic number of the impurity.

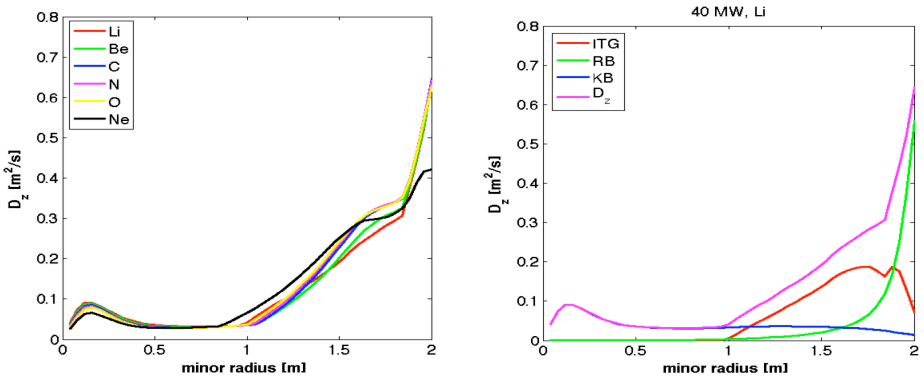

Figure 4. Radial profiles of average impurity diffusivity (D_Z) (left) and contributing terms of average impurity diffusivity (right) at steady state for Li, Be, C, N, O and Ne during the time 600 to 1000 s.

4. Conclusion

It is found that the impurity density and helium density rise and reach steady-state values in all scenarios. However, impurity in neon scenario appears to reach a steady state faster than the other impurities. The impurity density, helium density and temperature in a steady state decrease with an atomic number of impurity. On the other hand, the radiation loss and impurity transport in a steady state increase with an atomic number of impurity. Moreover, it is also found that the kinetic-ballooning term (KB) provides the largest contribution in the center of the plasma, the ITG term (ITG) provides the largest contribution in the region close to the center and the resistive ballooning contribution term (RB) provides the largest contribution near the edge of the plasma in all scenarios.

References

1. R.P. Doerner et al., Phys. Scr., 2004, **75**, T111.
2. K. Ohya, Phys. Scr., 2006, **70**, T124.
3. R.P. Drake, J. Nucl. Energy C, 1963
4. L. Daniel, Plasma Physics. Princeton University, 2012.
5. J. Schweinzer et al., Nucl. Fusion, 2011, **51**, 113003.
6. M.N.A. Beurskens et al., Nucl. Fusion, 2008, **48**, 095004.
7. Z. Yong-Zhen et al., Chin. Phys. B, 2009, **18**, 5406.
8. C E. Singer et al., Comput. Phys. Commun., 1988, **49**, 275-398
9. T. Onjun et al., Nucl. Fusion, 2009, **49**, 075003.
10. D. Hannum et al., Phys. Plasmas, 2001, **8**, 964-974.
11. G. Bateman et al., Phys. Plasmas, 1998, **5**, 1793-99.
12. W A. Houlgerg et al., P Phys. Plasmas, 1997, **4**, 3231.